Open access • Journal Article • DOI:10.1364/OL.44.003976

Polarization-insensitive silicon nitride arrayed waveguide grating — Source link

Qi Han, Jonathan St-Yves, Yuxuan Chen, Michael Menard ...+1 more authors

Institutions: Laval University, Université du Québec à Montréal

Published on: 15 Aug 2019 - Optics Letters (Optical Society of America)

Topics: Arrayed waveguide grating, Polarization mode dispersion, Orthogonal polarization spectral imaging, Polarization (waves) and Channel spacing

Polarization-insensitive silicon nitride arrayed waveguide grating

Qi Han, Jonathan St-Yves, Yuxuan Chen, Michaël Ménard, and Wei Shi

OSA Optics Letters, (Volume 44, Issue 16) (2019)

Doi: 10.1364/OL.44.003976

https://doi.org/10.1364/OL.44.003976

Polarization-insensitive silicon nitride arrayed waveguide grating

Qi Han,[1] Jonathan St-Yves,[1] Yuxuan Chen,[1] Michaël Ménard,[2] and Wei Shi[1,*]

[1]Centre d'optique, photonique et laser (COPL) and Département de génie électrique et génie informatique, Université Laval, 2375 rue de la Terrasse, Québec G1V 0A6, Canada
[2]Microtechnology and Microsystems Laboratory, Université du Québec à Montréal, 8888 succursale Centre-ville Montréal, Québec H3C 3P8, Canada
*Corresponding author: wei.shi@gel.ulaval.ca

Next-generation passive optical networks require integrated, polarization-insensitive wavelength-division multiplexing solutions, for which the recently emerging low-loss silicon nitride nanophotonic platforms hold great potential. A novel polarization-insensitive arrayed waveguide grating (AWG) built with silicon nitride waveguides is presented in this Letter. Polarization insensitivity is obtained when both the channel spacing and the center wavelength of the two orthogonal polarization states (i.e., the TE and TM waveguide modes) are simultaneously aligned. In our design, the channel spacing alignment between the polarization states is obtained by optimizing the geometry of the arrayed waveguides, whereas the central wavelength polarization insensitivity is obtained by splitting the two polarization states and adjusting their angle of incidence at the input star coupler to compensate for the polarization mode dispersion of the AWG. A 100 GHz 1 × 8 wavelength-division multiplexer with crosstalk levels below −16 dB is demonstrated experimentally.

Polarization-insensitive multiplexers and demultiplexers are crucial for wavelength-division multiplexed (WDM) optical links using standard single mode fibers. Arrayed waveguide gratings (AWGs) are among the most important devices in dense WDM (DWDM) systems. One approach to reduce the polarization sensitivity of AWGs reported previously [1] is based on using square waveguides in the array. However, this approach is limited, since the signal still suffers from polarization dispersion in the free-propagation regions (FPR) (i.e., the input and output star couplers). As a result, the channel spacing depends on the polarization state. Thus, complete polarization insensitivity can be difficultly obtained by simply using squared arrayed waveguides. Another solution that has been demonstrated is to insert a quarter-wave plate in the arrayed waveguides to eliminate the optical path difference between the TE and TM modes [2,3]. However, the addition of the quarter-wave plate might cause extra loss. Converting one of the input polarizations using a polarization splitter and rotator (PSR) before the AWG is an efficient method to achieve a polarization-insensitive demultiplexer [4], but it requires a more complex fabrication process to create an asymmetric waveguide, and it increases insertion losses.

Many AWGs have been reported on silicon-on-insulator (SOI) platforms [5–9]. These AWGs are appealing due to their small footprints. However, the high refractive index difference between the waveguide core and cladding makes them sensitive to phase errors caused by fabrication variations. Thin-film silicon nitride (SiN) AWGs fabricated with a SiO_2 cladding have some advantages over SOI [10–14]. SiN has a refractive index close to 2.0 at a wavelength of 1550 nm, which is much smaller than that of silicon. Therefore, SiN waveguides and devices are expected to have a better tolerance to fabrication errors. Moreover, SiN can be deposited by low-pressure chemical vapor deposition (LPCVD), giving it better optical characteristics at the expense of higher levels of stress, or by plasma enhanced chemical vapor deposition (PECVD), which results in higher propagation losses, but is a process prevalent in complementary metal–oxide–semiconductor (CMOS) foundries [15].

In this Letter, we propose and experimentally demonstrate a polarization-insensitive AWG in SiN for DWDM with 100 GHz channel spacing.

A microscope image of a fabricated prototype of the proposed AWG is shown in Fig. 1(a). Without loss of generality, we discuss its operating principle by considering only the demultiplexing operation. A main difference between this design and a conventional AWG is that the TE and TM modes are launched at different angles in the input star coupler, as shown in Fig. 1(c), to compensate for the phase mismatch between the TE and TM polarization states [16]. An on-chip polarization beam splitter is used to separate the two orthogonal polarization states, which can be realized using a directional coupler [17], as shown in Fig. 1(b). To obtain polarization-insensitive operation, both the channel spacing and the center wavelength should be polarization independent. This is achieved by (1) choosing an appropriate geometry for the arrayed waveguides (i.e., the waveguide width for a given thickness) and output star coupler, which ensures polarization-insensitive channel spacing and (2) calculating the angle required between the TE and TM input ports to make the central wavelength

National Science and Engineering Research Council of Canada (NSERC) Funding: CRDPJ 499664

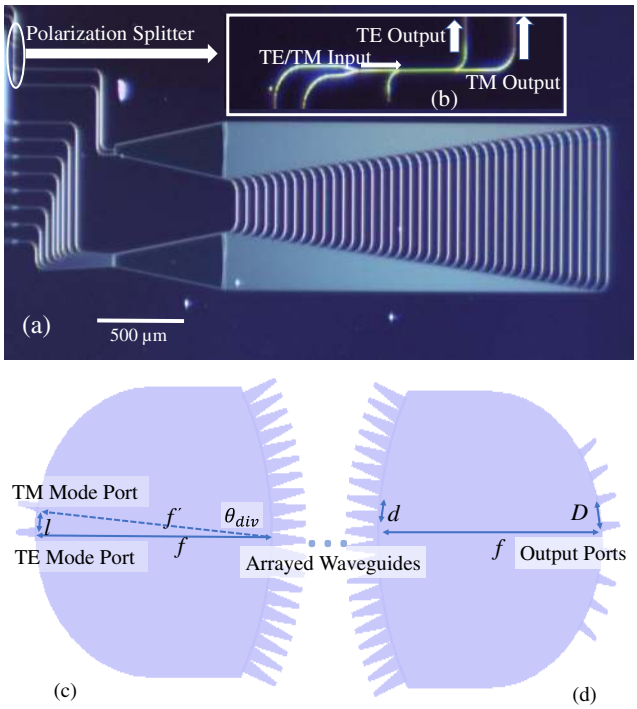

Fig. 1. (a) Microscope image of the polarization-insensitive AWG; (b) microscope image of the polarization beam splitter; (c) schematics of the input star couplers with different injection angles for TE and TM modes; (d) schematic of the output star coupler (not in scale).

polarization-insensitive. The mathematical principles are detailed below.

We first consider the channel spacing, which is determined by the design of the output star coupler and the arrayed waveguides. A schematic of the output star coupler is shown in Fig. 1(d), and the relationship between the channel spacing and the geometry of the coupler is given by [14,18]

$$\Delta\lambda = \frac{Dd n_s}{f m}, \tag{1}$$

where d is the separation between the arrayed waveguides, D is the separation between output waveguides, f is the length of the FPR, n_s is the effective index of the slab waveguide used to form the star coupler, m is the grating order, and $\Delta\lambda$ is the channel spacing of the AWG. In our design, we use a thickness for the SiN layer of 436 nm, determined by the wafer used in our fabrication process.

To compensate the channel spacing mismatch, we have to consider the impact of polarization mode dispersion (in both the effective and group indices) in the arrayed waveguides on the free spectral range (FSR) of the AWG. The channel spacing is chosen as $1/N$ of the FSR and given by [14]

$$\mathrm{FSR} = \frac{\lambda n_{\mathrm{eff}}}{m n_g} = N\Delta\lambda \Rightarrow \Delta\lambda = \frac{\lambda n_{\mathrm{eff}}}{m n_g}\frac{1}{N}, \tag{2}$$

where n_{eff} is the effective index of the arrayed waveguides, N is the output channels of the AWG, and n_g is the group index.

The channel spacing derived from the geometry of the output star coupler [Eq. (1)] needs to match the one of the arrayed waveguides [Eq. (2)]. From Eqs. (1) and (2), we can find that the effective index of the slab waveguide must be proportional to the ratio of the effective index to the group index of the arrayed waveguides:

$$\frac{Dd n_s}{f m} = \frac{\lambda n_{\mathrm{eff}}}{m n_g N} \Rightarrow n_s \propto \frac{n_{\mathrm{eff}}}{n_g}. \tag{3}$$

Polarization independent operation requires that $\frac{\Delta\lambda_{\mathrm{TE}}}{\Delta\lambda_{\mathrm{TM}}} = 1$, and thus, according to Eq. (3), the following condition must be met:

$$\frac{n_{\mathrm{eff,TE}}}{n_{g,\mathrm{TE}}} \Big/ \frac{n_{\mathrm{eff,TM}}}{n_{g,\mathrm{TM}}} = \frac{n_{s,\mathrm{TE}}}{n_{s,\mathrm{TM}}}. \tag{4}$$

To satisfy Eq. (4), the width of the arrayed waveguides has to be carefully designed. To simplify the discussion, we define two parameters referring to the left and right sides of Eq. (4): $\Gamma 1 = \frac{n_{s,\mathrm{TE}}}{n_{s,\mathrm{TM}}}$, $\Gamma 2 = \frac{n_{\mathrm{eff,TE}}}{n_{\mathrm{group,TE}}} / \frac{n_{\mathrm{eff,TM}}}{n_{\mathrm{group,TM}}}$. The effective index of the slab waveguide is calculated to be 1.75 and 1.67 for the TE and TM modes, respectively, giving $\Gamma 1 = 1.048$. To find a waveguide geometry where $\Gamma 2 = \Gamma 1$, we then calculated the effective and group indices of the SiN waveguide as function of the waveguide width using an Eigenmode solver. The waveguide thickness was kept constant at 436 nm. As shown in Fig. 2, $\Gamma 2$ increases with the waveguide width and equals $\Gamma 1$ at 371 nm, which is the value that has been adopted in our fabricated device.

We then consider the polarization response of the center wavelength. In order to achieve a polarization independent response, we need to align the focal points of both the TE and TM modes in the output star coupler. The center wavelength of the center channel is given by [19]

$$\lambda_{\mathrm{TE/TM}} = (n_{\mathrm{eff,TE/TM}}\Delta L - n_{s,\mathrm{TE/TM}} d l / f)/m_{\mathrm{TE/TM}}, \tag{5}$$

where ΔL is the length difference of adjacent arrayed waveguides, and l is the separation between the input ports, as shown in Fig. 1(c). In a conventional AWG design, the input port is set in the center of the star coupler for both polarization states (i.e., $l = 0$), and thus $\lambda_{\mathrm{TE/TM}} = n_{\mathrm{eff,TE/TM}}\Delta L/m_{\mathrm{TE/TM}}$. When both the TE and TM modes are launched into the same port, the relationship between the grating orders of the TE and TM modes is given by

$$\Delta L = \frac{m_{\mathrm{TE}}\lambda}{n_{\mathrm{eff,TE}}} = \frac{m_{\mathrm{TM}}\lambda}{n_{\mathrm{eff,TM}}} \Rightarrow m_{\mathrm{TM}} = \frac{m_{\mathrm{TE}} n_{\mathrm{eff,TM}}}{n_{\mathrm{eff,TE}}}. \tag{6}$$

For the waveguide geometry considered here, the ratio $n_{\mathrm{eff,TM}}/n_{\mathrm{eff,TE}} = 1.006$. As a result, it is impossible to obtain

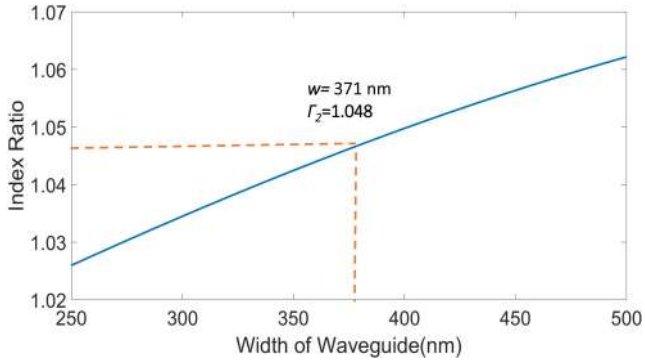

Fig. 2. Ratio ($\Gamma 2$) of the TE slab waveguide index ($n_{s,\mathrm{TE}}$) to the TM slab waveguide index ($n_{s,\mathrm{TM}}$) as a function of the width of the waveguide.

National Science and Engineering Research Council of Canada (NSERC) Funding: CRDPJ 499664

an integral grating order for both the TE and TM modes and achieve a polarization-insensitive response. For example, for $m_{\mathrm{TE}} = 125$, m_{TM} should be 125.75 according to Eq. (6) in order to obtain polarization independent operation. Otherwise, the TE and TM modes will be focused at different locations in the output star coupler.

To address this issue, we introduce an extra optical path to obtain an integer value for the TM mode grating order and simultaneously align the focal positions of both polarizations. In this design, we set the position of the TE mode input port at the center of the input star coupler (i.e., normal incidence). The TM mode input port is located at a distance l to the center of the star coupler, as shown in Fig. 1(c). We use a polarization splitter to separate the polarization states at the input before the first star coupler, as shown in Fig. 1(a). This approach was originally proposed in [16] but not demonstrated experimentally. An extra optical path length of $(f' - f)\, n_{s,\mathrm{TM}}$ is introduced for the TM mode, where f is the focal length of the center input port (i.e., the TE mode), and f' is the focal length for the TM mode. As a result, the central wavelengths of operation are the same for both the TE and TM modes. The angle (θ_{div}) required between the inputs is given by [19]

$$\theta_{\mathrm{div}} = \frac{l}{f} = (n_{s,\mathrm{TM}} n_{\mathrm{eff,TE}} \Delta L - n_{s,\mathrm{TE}} n_{\mathrm{eff,TM}} \Delta L)/n_{s,\mathrm{TM}} n_{s,\mathrm{TE}} d. \tag{7}$$

To demonstrate this approach, we designed an eight-channel polarization-insensitive AWG with a center wavelength of 1550 nm and a channel spacing of 100 GHz. As described above, the arrayed waveguides have a rectangular strip waveguide geometry with a thickness of 436 nm and a width of 371 nm. The angle between the TE and TM inputs is set to 2.79°, and the grating orders for the TE and TM modes are 125 and 131, respectively. The separation between the arrayed waveguides is 6.4 μm, the separation between output waveguides is 10.2 μm, and the length of the FPR is 1142.5 μm in the output star coupler. Forty arrayed waveguides separated by at least 10 μm are used in the device. In order to minimize bending losses, a large bending radius of 100 μm is used to implement the array. Figure 1 shows the entire device.

The device was fabricated using e-beam lithography and dry etching to pattern a layer of SiN formed on 4 μm of SiO_2; then, a top cladding of 4 μm SiO_2 was deposited. Light is coupled to the chip through surface grating couplers (SGCs). Since the SGCs are efficient for only one polarization, two different designs of SGCs (one for the TE mode and the other for the TM mode) combined by a Y branch are used for each input/output waveguide of the AWG. Their responses are calibrated using a pair of the same Y-branch-combiners connected by a short waveguide on the same chip. The fabricated polarization-insensitive AWG is characterized using an automated measurement setup equipped with TE and TM sources.

The layout of the polarization splitter, which is an asymmetric directional coupler, is shown in Fig. 3 [a microscope image of the fabricated device is shown in Fig. 1(b)]. It consists of two strip waveguides with different widths. The TE mode propagates through the input waveguide, while the TM mode is coupled into the cross port. The coupling length is 130 μm, the width of the waveguides is 900 nm, and the gap in the coupler is 0.59 μm. The measured excess loss is 1 dB for the TE mode and approximately 1.5 dB for the TM mode.

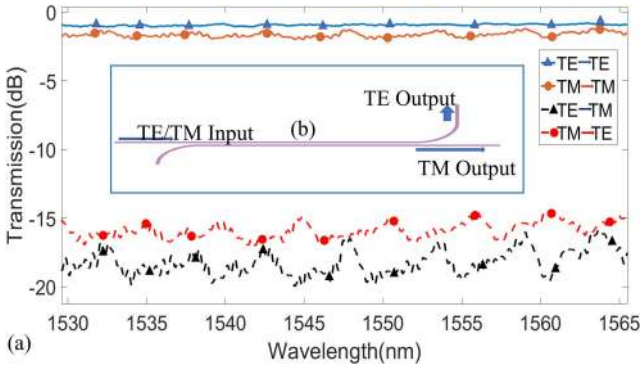

Fig. 3. (a) Measured power transmission spectra of the polarization beam splitter for the TE and TM modes; (b) layout schematic of the polarization beam splitter.

The best crosstalks are −18 dB at the TE output port and −16 dB at the TM output port.

Figure 4 shows the normalized transmission spectrum of the fabricated polarization-insensitive AWG. The blue curve shows the spectrum of the TE mode, and the red curve shows the spectrum of the TM mode. At the central wavelength, an insertion loss of approximately −6 dB is measured for the TE mode and −6.2 dB for the TM mode. The insertion loss of the AWG includes the waveguide scattering loss, the bending loss in the arrayed waveguides, and the transition coupling loss between the star couplers and the arrayed waveguides. The bending loss of the arrayed waveguides can be decreased by utilizing a larger bend; however, excess insertion loss will be introduced due to a larger overall waveguide length. Furthermore, tapered waveguides are used at the junctions between the arrayed waveguides and the star couplers in order to minimize transition loss. Nevertheless, scattering losses in the fabricated device are important due to the roughness of the sidewall. The measured propagation loss is about 1.5 dB/cm for straight waveguides. The total insertion loss could be significantly reduced by improving the reactive ion etching process.

The crosstalk across all eight channels of the AWG ranges from −16 to −20 dB. It is related to the resolution of the recombined field distribution at the output waveguides. This resolution is a function of the number of optical delay waveguides; a larger number results in a more faithful recreation of

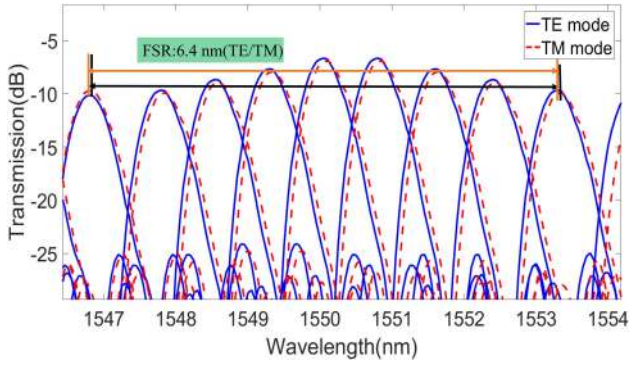

Fig. 4. Measured power transmission spectra of the AWG for the TE and TM polarizations.

National Science and Engineering Research Council of Canada (NSERC) Funding: CRDPJ 499664

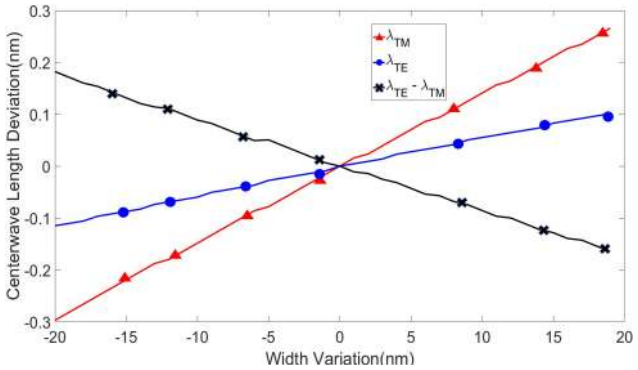

Fig. 5. Simulated center wavelength deviations due to fabrication errors in waveguide width.

the input image. However, it also leads to a larger footprint and increases the probability of phase errors in the fabrication process. Thus, there is an optimum number of waveguides for which the level of crosstalk is minimized, beyond which phase errors overcome the gain in resolution provided by increasing the number of waveguides. As a rule of thumb, the number of arrayed waveguides should be about 3.5 times the number of output channels [20].

As shown in Fig. 4, the measured channel spacing is 0.8 nm (100 GHz) with an FSR of 6.4 nm for both the TE and TM modes, as expected. This proves that we achieved polarization insensitivity in the channel spacing through optimizing the geometry of arrayed waveguides. However, the center wavelengths of the TE and TM modes do not match perfectly with each other. The center wavelength is 1550.05 nm for the TE mode and 1550.15 nm for the TM mode. We attribute this deviation to fluctuations in the width of the waveguides due to fabrication errors. Assuming a good uniformity in thickness, we calculated the center wavelength deviation as a function of the variation in width of the waveguides, as shown in Fig. 5. The variation of the width of the waveguides affects the center wavelength of the AWG by changing the effective index of the arrayed waveguides. We can see that a width variation of 12 nm causes a drift in the center wavelength by 0.1 nm. This difference in center wavelength between the two polarization states could by reduced by improving the fabrication process or adopting a flat-top AWG design [21].

In summary, we presented a design methodology to obtain a polarization-insensitive AWG that combines two techniques. First, the effective and group indices of the TE and TM modes are engineered by optimizing the geometry of the arrayed waveguides to achieve an identical FSR for both orthogonal polarization states. Then, to align the central wavelength of each channel for both polarizations, the TE and TM modes are separated into two different waveguides via an on-chip polarization splitter. Each polarization state is launched into the first star coupler of the AWG with a different angle of incidence that allows it to compensate for the polarization dispersion of the AWG. Following this methodology, we realized a 1×8 DWDM AWG with SiN waveguides using a CMOS-compatible fabrication process. We achieved a channel spacing of 100 GHz for both polarization states with a crosstalk below −16 dB. The remaining deviation of 0.1 nm in the central wavelength between the TE and TM modes could be compensated for through further optimization of the fabrication process. Our results show that SiN is promising for the implementation of AWGs targeting DWDM applications, such as a WDM passive optical network (WDM-PON), where a low-cost polarization-insensitive WDM solution is required.

Funding. Natural Sciences and Engineering Research Council of Canada (CRDPJ 499664); Mitacs; Aeponyx Inc. (Canada); TELUS Corp; PROMPT Québec (Canada).

Acknowledgment. We thank the AEPONYX Inc. team for many useful discussions. This research was funded by Mitacs, AEPONYX Inc., TELUS Corp., PROMPT Québec, and the Natural Sciences and Engineering Research Council of Canada.

REFERENCES

1. M. R. Amersfoort, J. B. D. Soole, H. P. LeBlanc, N. C. Andreadakis, A. Rajhel, C. Caneau, M. A. Koza, U. Bhat, and C. Youtsey, *Optical Fiber Communications (OFC '96)* (1996), Vol. **2**, p. WB5.
2. C. Nadler, E. Wildermuth, M. Lanker, W. Hunziker, and H. Melchior, IEEE J. Sel. Top. Quantum Electron. **5**, 1407 (1999).
3. H. Takahashi, Y. Hibino, and I. Nishi, Opt. Lett. **17**, 499 (1992).
4. C. Long, C. R. Doerr, and Y.-K. Chen, Opt. Lett. **36**, 469 (2011).
5. P. Trinh, S. Yegnanarayanan, F. Coppinger, and B. Jalali, IEEE Photon. Technol. Lett. **9**, 940 (1997).
6. K. Jia, W. Wang, Y. Tang, Y. Yang, J. Yang, X. Jiang, Y. Wu, M. Wang, and Y. Wang, IEEE Photon. Technol. Lett. **17**, 378 (2005).
7. P. Dumon, W. Bogaerts, D. V. Thourhout, D. Taillaert, R. Baets, J. Wouters, S. Beckx, and P. Jaenen, Opt. Express **14**, 664 (2006).
8. S. Cheung, T. Su, K. Okamoto, and S. J. B. Yoo, IEEE J. Sel. Top. Quantum Electron. **20**, 8202207 (2014).
9. P. Cheben, J. H. Schmid, A. Delâge, A. Densmore, S. Janz, B. Lamontagne, J. Lapointe, E. Post, P. Waldron, and D. Xu, Opt. Express **15**, 2299 (2007).
10. J. F. Bauters, J. R. Adleman, M. J. R. HeckJohn, and E. Bowers, Appl. Phys. A **116**, 427 (2014).
11. D. Martens, A. Z. Subramanian, S. Pathak, M. Vanslembrouck, P. Bienstman, W. Bogaerts, and R. G. Baets, IEEE Photon. Technol. Lett. **27**, 137 (2015).
12. C. R. Doerr, L. Chen, L. L. Buhl, and Y.-K. Chen, IEEE Photon. Technol. Lett. **23**, 1201 (2011).
13. L. Chen, C. R. Doerr, L. Buhl, Y. Baeyens, and R. A. Aroca, IEEE Photon. Technol. Lett. **23**, 869 (2011).
14. P. Gatkine, S. Veilleux, Y. Hu, T. Zhu, Y. Meng, J. Bland-Hawthorn, and M. Dagenais, Opt. Express **25**, 17918 (2017).
15. A. Rahim, E. Ryckeboer, A. Subramanian, S. Clemmen, B. Kuyken, A. Dhakal, A. Raza, A. Hermans, M. Muneeb, S. Dhoore, Y. Li, U. Dave, P. Bienstman, N. L. Thomas, G. Roelkens, D. V. Thourhout, P. Helin, S. Severi, X. Rottenberg, and R. Baets, J. Lightwave Technol. **35**, 639 (2017).
16. M. K. Smit and C. van Dam, J. Sel. Top. Quantum Electron. **2**, 236 (1996).
17. H. Fukuda, K. Yamada, T. Tsuchizawa, T. Watanabe, H. Shinojima, and S. I. Itabashi, Opt. Express **14**, 12401 (2006).
18. H. Sattari, Optik **123**, 775 (2011).
19. A. Kaneko, T. Goh, H. Yamada, T. Tanaka, and L. Ogawa, IEEE J. Sel. Top. Quantum Electron. **5**, 1227 (1999).
20. S. Pathak, P. Dumon, D. V. Thourhout, and W. Bogaerts, IEEE Photon. J. **6**, 5710 (2014).
21. S. Pathak, M. Vanslembrouck, P. Dumon, D. V. Thourhout, and W. Bogaerts, J. Lightwave Technol. **31**, 87 (2013).